



**UNIVERSITY OF LEEDS**

This is a repository copy of *On the injectability of free-standing magnetic nanofilms*.

White Rose Research Online URL for this paper:

<http://eprints.whiterose.ac.uk/116749/>

Version: Accepted Version

---

**Article:**

Taccola, S, Pensabene, V [orcid.org/0000-0002-3352-8202](https://orcid.org/0000-0002-3352-8202), Fujie, T et al. (3 more authors) (2017) On the injectability of free-standing magnetic nanofilms. *Biomedical Microdevices*, 19. 51. ISSN 1387-2176

<https://doi.org/10.1007/s10544-017-0192-1>

---

© Springer Science+Business Media New York 2017. This is an author produced version of a paper published in *Biomedical Microdevices*. The final publication is available at Springer via <https://doi.org/10.1007/s10544-017-0192-1>. Uploaded in accordance with the publisher's self-archiving policy.

**Reuse**

Items deposited in White Rose Research Online are protected by copyright, with all rights reserved unless indicated otherwise. They may be downloaded and/or printed for private study, or other acts as permitted by national copyright laws. The publisher or other rights holders may allow further reproduction and re-use of the full text version. This is indicated by the licence information on the White Rose Research Online record for the item.

**Takedown**

If you consider content in White Rose Research Online to be in breach of UK law, please notify us by emailing [eprints@whiterose.ac.uk](mailto:eprints@whiterose.ac.uk) including the URL of the record and the reason for the withdrawal request.



[eprints@whiterose.ac.uk](mailto:eprints@whiterose.ac.uk)  
<https://eprints.whiterose.ac.uk/>

# On the injectability of free-standing magnetic nanofilms

*Silvia Taccola\**,<sup>‡</sup> *Virginia Pensabene*,<sup>‡,1</sup> *Toshinori Fujie*,<sup>†φ</sup> *Shinji Takeoka*,<sup>§</sup> *Nicola M. Pugno*,  
<sup>a,b,c</sup> *Virgilio Mattoli*<sup>\*‡</sup>

<sup>‡</sup>Center for MicroBioRobotics IIT@SSSA, Istituto Italiano di Tecnologia, Viale Rinaldo Piaggio  
34 Pontedera, 56025 (Italy), <sup>†</sup>Waseda Institute for Advanced Study, Waseda University, TWIns,  
2-2 Wakamatsu-cho, Shinjuku-ku, Tokyo, 162-8480 (Japan), <sup>φ</sup>Japan Science and Technology  
Agency, PRESTO, 4-1-8 Honcho, Kawaguchi, Saitama, 332-0012 (Japan), <sup>§</sup>Department of Life  
Science and Medical Bioscience, Graduate School of Advanced Science and Engineering,  
Waseda University, TWIns, 2-2 Wakamatsu-cho, Shinjuku-ku, Tokyo 162-8480 (Japan),  
<sup>a</sup>Laboratory of Bio-Inspired & Graphene Nanomechanics, Department of Civil, Environmental  
and Mechanical Engineering, University of Trento, Via Mesiano 77, 38123 Trento, Italy, <sup>b</sup>School  
of Engineering and Materials Science, Queen Mary University of London, Mile End Road, E1  
4NS London, United Kingdom, <sup>c</sup>Italian Space Agency, Via del Politecnico snc, 00133 Rome,  
Italy.

## Corresponding Author

\* Tel:+39-050-883414, Fax: +39-050-883101, E-mail: [silvia.taccola@iit.it](mailto:silvia.taccola@iit.it),  
[virgilio.mattoli@iit.it](mailto:virgilio.mattoli@iit.it).

## Present Addresses

<sup>1</sup>Virginia Pensabene, School of Electronic and Electrical Engineering, University of Leeds, Woodhouse Lane, LS2 9JT, Leeds, UK <sup>3</sup>School of Medicine, Leeds Institute of Biomedical and Clinical Sciences, University of Leeds, Woodhouse Lane, LS2 9JT, Leeds, UK

**ABSTRACT:** Free-standing films with sub-micrometric thickness, composed of soft polymers and functional nanostructures are promising candidates for many potential applications in the biomedical field, such as reduced port abdominal surgery. In this work, freely suspended poly(L-lactic acid) nanofilms with controlled morphology embedding superparamagnetic iron oxide nanoparticles were fabricated by spin-coating deposition. The mechanical properties of magnetic nanofilms were investigated by Strain-Induced Elastic Buckling Instability for Mechanical Measurements (SIEBIMM) test. Our results show that these freely suspended nanocomposite nanofilms are highly flexible and deformable, with Young's moduli of few GPa. Since they can be handled in liquid with syringes, a quantitative description of the nanofilms behavior during the manipulation with clinically applicable needles has been also provided. These magnetic nanofilms, remotely controllable by external electromagnetic fields, have potential applications in minimally invasive surgery as injectable nanopatches on inner organs wall.

**Key Words:** nanofilm; nanopatch; injectability; magnetic nanocomposite; SIEBIMM; minimally invasive surgery.

## 1. INTRODUCTION

Recent developments in the field of nanotechnology have led to the realization of free-standing nanostructured ultrathin polymeric films (also called “nanofilms”), which are

characterized by an aspect ratio of size and thickness greater than  $10^6$  (size in the order of centimeter and tens-of-nanometers thickness) (Jiang 2006, Ono 2006, Tang 2006, Mamedov 2000). The combination of nanometer thickness and macroscopic size imparts to these quasi-two-dimensional (2-D) structures unique physical properties, such as high flexibility, transparency and noncovalent adhesiveness. Moreover, the integration of functional nanostructures, such as magnetic nanoparticles, gold nanoparticles, and carbon nanotubes, into the polymeric matrix, as well as the use of functional polymers, can bestow high-performance nanofilms of new magnetic, optical, mechanical, or electronic properties (Fujie 2016, Jiang 2004, Mamedov 2002, Redolfi Riva 2014, Greco 2011). Free-standing polymeric nanofilms have been fabricated using different approaches, including Langmuir-Blodgett (Endo 2006), layer-by-layer (LbL) (Decher 1997), dip-coating (Tang 2006), sol-gel (Vendamme 2006) and spin-coating method (Okamura 2009). Up to date, nanofilms have been investigated for applications in nano-electronics, nano/micro sensing and actuation devices, electrochemical devices, nanoscale chemical and biological reactors, drug-delivery systems and as ultra-conformable electrodes (Kang 2008, Redolfi Riva 2013, Taccola 2013, Zucca 2015).

Recently, biodegradable and biocompatible materials (e.g. polysaccharides or polyesters) have been proposed as soft patches for cosmetic use, as innovative alternative to traditional surgical sutures, as nanopatches on gastrointestinal wall or as flexible cell growth supports (Okamura 2009, Fujie 2007, Fujie 2009, Pensabene 2009, Ricotti 2010, Fujie 2011, Fujie 2012, Ventrelli 2014, Fujie 2014). In particular, it has been demonstrated that free-standing poly(L-lactic acid) (PLLA) nanofilms can adhere tightly to skin or organs by physical adhesion (i.e. van der Waals interaction) and have an excellent sealing effect on the closure of gastric incisions as a wound dressing that requires no adhesive agents (Okamura 2009, Pensabene 2009).

In this framework, the concept of nanofilms as “nano-adhesive plasters” for wound repair can become extremely appealing in the field of minimally-invasive surgery, combining the adhesive properties of PLLA nanofilms with the ability of these flexible structures to be easily manipulated with syringes and pipettes, injecting and ejecting multiple times without distortion. Thus, the PLLA nanofilms could be injected inside the human body in different fluids and spaces employing a small catheter or a plastic cannula, or directly through the working channel of an endoscope and then used as nanopatches on inner organ walls. For example, nanofilms could be employed in endoscopic or laparoscopic surgery for localized thermal ablation procedures (Baker 2006), as a new method for surface ferromagnetisation of tissues (Wang 2014), as surface marking of localized small lesions discovered during endoscopic examinations (Wang 2016).

Recently polymeric biocompatible glues have been loaded with ferromagnetic particles to be used as novel tools for magnetic grasping (Wang 2008), as distinct from pull retraction, in conjunction with an adjustable magnetic force system deployed inside the abdominal cavity or outside the body. Polymeric mucoadhesive films were instead synthesized with the final aim to anchor permanent magnets onto the abdominal and intestinal serial surfaces to enable magnetic tissue retraction during reduced port surgery (Pensabene 2011). This approach enabled long term anchoring of surgical assistive tools in an endoscopic procedure, but could not guarantee stable adhesion on wet tissues during multidirectional magnetic retraction.

Herein, we envisaged to develop a biocompatible polymeric nanofilm, which could be remotely manipulated and positioned onto the stomach incision site precisely by using minimal-invasive external tools. The integration of magnetic components into PLLA nanofilms represents the first step for the development of magnetic nanofilms with the potential of a remote-controlled manipulation by permanent and gradient magnetic fields, as already

theoretically and experimentally demonstrated (Mattoli 2010, Taccola 2011). The use of magnetic fields to remotely control microdevices in narrow and delicate districts and apparatus of the human body is a well-accepted approach nowadays in surgical and diagnostic procedures, where remote-magnetic navigation catheters or magnetic robotic capsules are finely controlled by coupling with permanent magnetic fields (Ciuti 2010). Free-standing polymeric nanofilms composed of poly(L-lactic acid) (PLLA), embedding superparamagnetic iron oxide nanoparticles (SPIONs), were successfully fabricated in our laboratory and their morphological and magnetic properties have been characterized (Taccola 2011). In this study, we focused on the biomedical application of magnetic nanofilms as injectable nanopatches, and evaluated their mechanical properties and “injectability” through clinically applicable syringes and needles (See Figure 1). In particular, the “injectability” was defined as the ability of the magnetic nanofilm to pass through a needle without distortion, and was experimentally evaluated by varying the lateral size of the nanofilms and SPIONs concentrations with respect to syringe needle of different inner diameters. Finally we successfully introduced an analytical model able to predict the injectability of nanofilm at given syringe needle diameter.

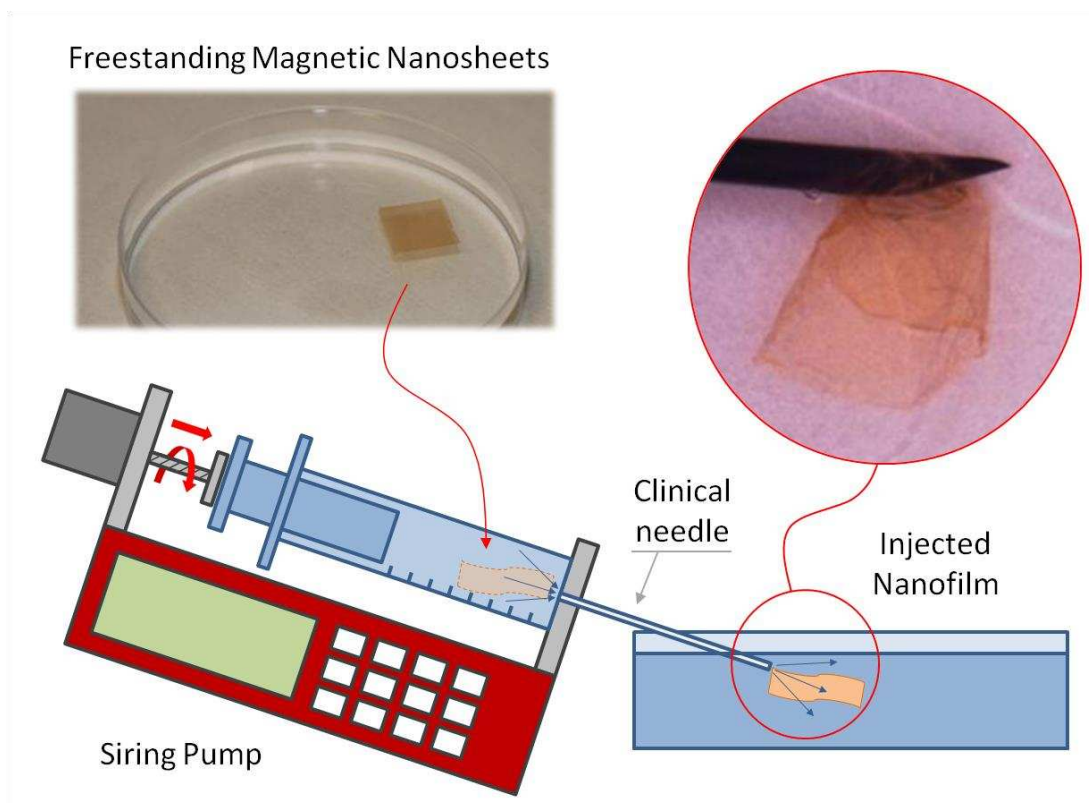


**Figure 1.** Overview of the experimental framework used for the evaluation of nanofilms injectability vs. geometrical and composition features.

## 2. MATERIALS AND METHODS

**Materials.** Silicon wafers (400  $\mu\text{m}$  thick, p type, boron doped, <100>, Si-Mat Silicon Materials, Kaufering, Germany), used as substrates for film deposition, were cut (2 cm  $\times$  2 cm) and treated using an acid washing solution (SPM: 96 %:30 %  $\text{H}_2\text{SO}_4/\text{H}_2\text{O}_2 = 4:1$  (v/v)) at 120  $^\circ\text{C}$  for 10 min and then thoroughly rinsed with deionized (DI) water (18  $\text{M}\Omega$  cm) in order to remove dust and impurities. Poly(vinyl alcohol) (PVA, average Mw 13,000-23,000, 98 % hydrolyzed) was purchased from Kanto Chemical Co., Inc. (Tokyo, Japan). Poly(L-lactic acid) (PLLA, Mw 80,000-100,000) was obtained from Polysciences Inc. (Warrington, PA). Commercially available

superparamagnetic magnetite/maghemite nanoparticles with a polymeric coating layer (EMG1300), having a nominal diameter of 10 nm, were purchased from FerroTec Co. (San Jose, CA).

**2.1 Fabrication of single layer PLLA and PLLA-SPIONs nanofilms.** Free-standing magnetic PLLA nanofilms and unloaded PLLA nanofilms (used as a control for characterization) were prepared by spin coated assisted deposition following the procedure described in details elsewhere (Taccola 2011). Briefly, a PVA aqueous solution (1 wt%) was deposited by spin-coating on a silicon wafer (at 4000 rpm for 20 s) forming a water-soluble sacrificial layer. A stable colloidal solution of SPIONs and PLLA in chloroform (PLLA 1 wt%) was then spin-coated on the sacrificial layer by using the same spinning parameters. After each step, the sample was held at 80 °C on a hot plate for 1 min to remove the excess solvent. Finally, the polymer-coated wafer was immersed in water: the PVA sacrificial layer was dissolved, thus releasing a freely suspended insoluble PLLA nanofilm. All routines for PLLA nanofilms fabrication were conducted in a clean room (class 10000) to avoid contamination. In this study, different PLLA nanofilms were prepared by varying the number of nanoparticles added to the solution. The samples were referred as PL10-SP $x$ , denoting films prepared using 10 mg mL<sup>-1</sup> PLLA and  $x$  mg mL<sup>-1</sup> SPIONs colloidal solutions ( $x = 0, 1, 5, 10, 15$ ).

## **2.2 Characterization of mechanical properties.**

Silicon wafers (400  $\mu$ m thick, p-type, boron doped, <100>, Si-Mat Silicon Materials) were silanized by placing them in a desiccator for 30 min along with a vial that contained a few drops of silanizing agent (chlorotrimethylsilane, Sigma–Aldrich). The PDMS substrate was prepared at a 10:1 ratio by weight of base elastomer to curing agent. The mixture, after the release of entrapped air bubbles in a vacuum bell desiccator was spin-coated onto the silanized Si

substrates for 60 s at a speed of 200 rpm and then cured at  $T = 95\text{ }^{\circ}\text{C}$  for 60 min in an oven. The cured PDMS was cut into slabs ( $4 \times 2\text{ cm}^2$ ). Nanofilms were released into water, and collected on a prestretched ( $\sim 5\%$  strain of the original size) PDMS substrate. The samples were dried overnight prior to the Strain-Induced Elastic Buckling Instability for Mechanical Measurements (SIEBIMM) test. The strain of the PDMS substrate was then relaxed, producing the buckling of the nanofilm. The buckling wavelength of the nanofilm was measured by Atomic Force Microscope (AFM) imaging, using a Veeco Innova Scanning Probe Microscope (Veeco Instruments Inc., Santa Barbara, CA) operating in tapping mode, with a RTESPA Al-coated silicon probe (Veeco Instruments Inc.). The formula used to calculate the Young's modulus of the nanofilm is reported as Equation 1 in this paper.

**2.3 Injectability test.** The capability of nanofilms to be manipulated without breaking through syringes equipped with clinically applicable needles (Terumo Medical Corporation, Elkton, MD, USA, needles inlet diameter 1.1 mm, 0.9 mm, 0.6 mm, 0.45 mm) has been experimentally investigated and quantified by the parameter  $I$  ("injectability"). Due to their hydrophobicity, the manipulation of free-standing nanofilms in water was possible only after the addition of a PVA solution (0.1 wt %) in suspension medium, in which PVA was acting as a surfactant. Nanofilms were then inserted into the syringe filled with this solution and consequently forced through the needle by a constant pressure of 2.5 psi. A syringe pump was used in order to apply the constant pressure from the syringe piston.

For each SPIONs concentration, the injectability test was performed on square nanofilms having different lateral size (5, 7, 10, 12, 15, 17, 20, 22 and 25 mm). Each test was independently repeated 10 times using new samples, new needles and new solutions. The injectability test determined if a nanofilm can be successfully injected through a specified needle. Therefore, each

trial had only two possible outcomes: if the nanofilm could pass through the needle without distortion, the injection succeeded; if the nanofilm caused the clogging of the needle or was damaged during the passage through the needle, the injection failed. Then, the “injectability” parameter ( $I$ ) was measured as the number of success among 10 trials, expressed as a percentage.

The morphology of the nanofilms after the injection was evaluated on samples collected from the suspended state and dried on clean silicon wafers using optical microscopy, while scanning electron microscope (SEM) and atomic force microscopy (AFM) have been employed for identifying cracks, wrinkles or other discontinuities caused by the induced stresses. Optical images of the film surface were taken by using a Hirox KH7700 digital microscope (Hirox Co Ltd., Tokyo, Japan). AFM measurements were carried out on a Veeco Innova Scanning Probe Microscope (Veeco Instruments Inc., Santa Barbara, CA) operating in tapping mode, using an RTESPA Al-coated silicon probe (Veeco Instruments Inc.). SEM images were obtained using a Zeiss EVO/MA 10 field emission microscope (Carl Zeiss SMT, Oberkochen, Germany) at an acceleration voltage of 10 keV. Specimens for the SEM experiments were sputtered with a thin layer of gold before the observation.

### **3. RESULTS AND DISCUSSIONS**

**3.1 Preparation and characterization of magnetic nanofilms.** In our previous work, we developed free-standing and flexible PLLA nanofilms loaded with superparamagnetic nanoparticles in a simple, fast single-step deposition process (Taccola 2011). The effect of each production parameters (i.e. PLLA and SPIONs concentration in the deposited dispersion) on the morphological properties and magnetic behavior of nanofilms has been completely characterized (Taccola 2011). From this study, magnetic nanofilms fabricated from the spin coating of  $10 \text{ mg mL}^{-1}$  PLLA solutions appeared to be particularly suitable for the proposed application,

because of the good homogeneity of SPIONs dispersion and the  $\sim 100$  nm thickness, which was previously reported as key feature for an efficient adhesion on the mucosal tissue (Pensabene 2009). The physical properties of nanofilms obtained from a dispersion containing  $10 \text{ mg mL}^{-1}$  PLLA and different concentrations of SPIONs (0, 1, 5, 10, 15  $\text{mg mL}^{-1}$ ) were summarized in Table 1.

**Table 1.** Morphological and magnetic properties of  $10 \text{ mg mL}^{-1}$  PLLA and PLLA/SPIONs nanofilms (data from Taccola 2011).

Sample	Thickness (nm)	Roughness (nm)	Nanoparticles mass fraction in the composite (%)	Mass magnetic susceptibility ( $\text{cm}^3 \text{ g}^{-1}$ )
PL10-SP0	87±4	2.3	-	-
PL10-SP1	141±4	3.7	12.1	0.012
PL10-SP5	139±2	5	31.5	0.032
PL10-SP10	154±3	17.6 (118) <sup>a</sup>	47.5	0.048
PL10-SP15	205±8	31.2 (132.3) <sup>a</sup>	91.7	0.093

<sup>a</sup>Clusters' average equivalent disk radius (nm).

The thickness of the nanofilms, determined from AFM thickness measurements, increased with the number of SPIONs in the composite and varied in a range from 87 nm for PL10-SP0 to 205 nm for PL10-SP15. The magnetic behavior of nanofilms, could be described by superparamagnetic modeling, with the saturation magnetization depending only on the nanoparticles number density. The magnetization evaluation has been used to estimate the mass magnetic susceptibility of the nanofilms and the SPIONs mass fraction in the nanocomposite that are key factors in describing the magnetic guidance of the freely suspended nanofilms in liquid environment (Mattoli 2010, Taccola 2011).

As reported in Taccola 2011, a uniform distribution of SPIONs inside the polymeric matrix was evidenced via both AFM and transmission electron microscopy (TEM). It is noteworthy that, as the SPIONs concentration increased, the presence of particle clusters emerging from the surface of the samples was evident.

### **3.2 Mechanical properties of magnetic nanofilms.**

Mechanical properties free-standing nanofilms were evaluated SIEBIMM, a technique used for the determination of the Young's modulus of polymer ultrathin films [35]. This technique is based on measuring the wavelength  $\lambda$  of the periodic wrinkles formed on the buckled surface of polymer thin films coating a relatively soft, thick elastic substrate such as PDMS. If the elastomer substrate is pre-stretched, the relaxation of strain induces the buckling of the film. By applying buckling mechanics, the Young's modulus ( $E_n$ ) is obtained by using the following formula:

$$E_n = \frac{3(E_s(1-v_n^2))}{(1-v_s^2)} \left(\frac{\lambda}{2\pi t}\right)^3 \quad (1)$$

where  $E$  is the Young's modulus,  $v$  is the Poisson's ratio and  $n, s$  subscripts refer to nanofilm and substrate (PDMS), respectively. In Equation 1, we employed Young's modulus value of PDMS  $E_s = 1.8$  MPa, the Poisson's ratios of the nanofilm  $v_n = 0.33$  and of the PDMS  $v_s = 0.50$ , by following the Rubner's report (Stafford 2004). The wavelength was estimated by AFM analysis of wrinkled nanofilms, as showed in Figure 2A. By incorporating the measured wavelength  $\lambda$  into Equation 1 the Young's modulus of the nanofilms  $E_n$  was evaluated (Figure 2B,C).

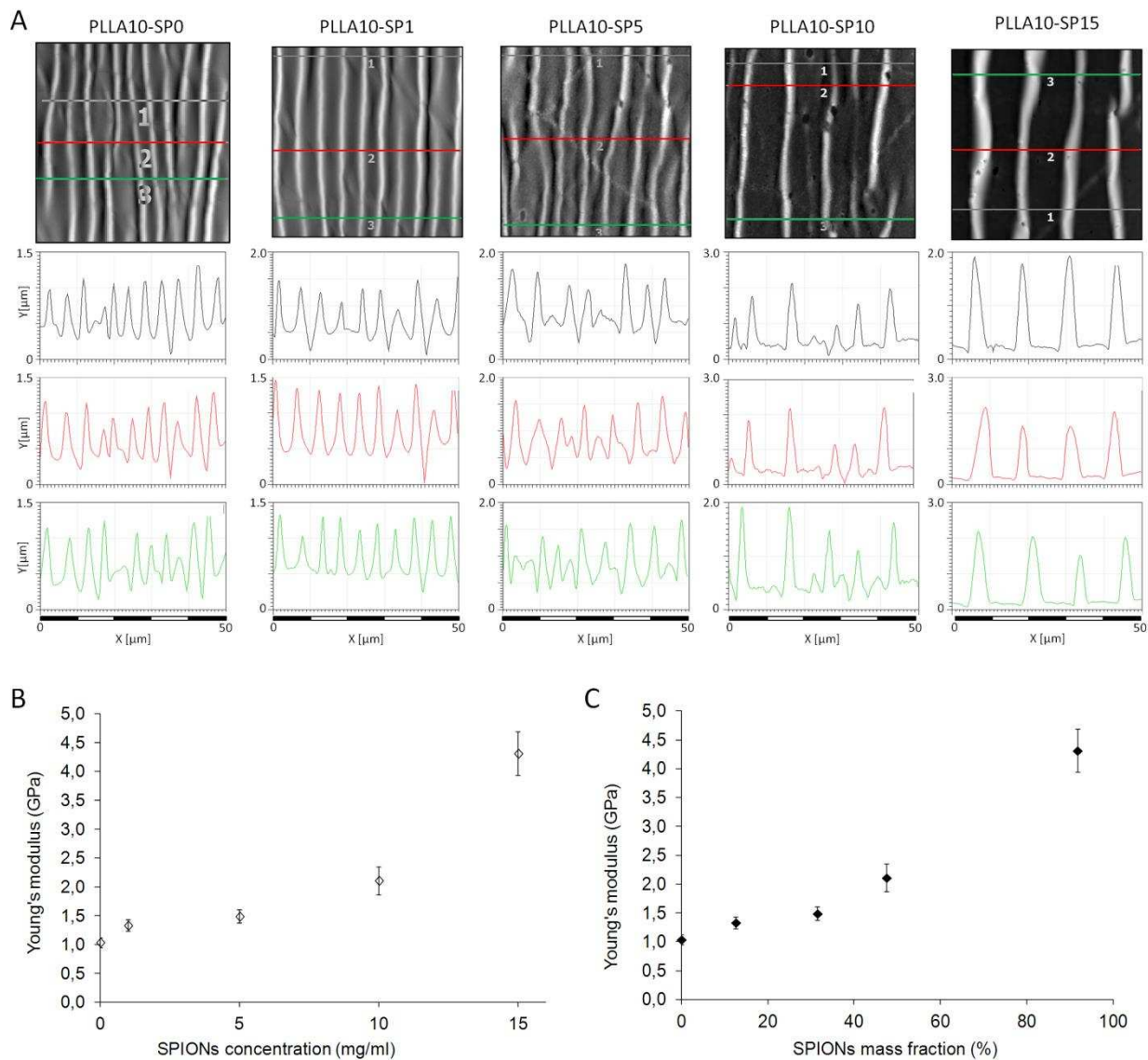


**Figure 2.** Mechanical properties of the PLLA nanofilms with different SPIONs concentrations evaluated by the SIEBIMM measurement. A) AFM images of wrinkled nanofilms and relative surface profiles used to estimate the wavelength (defined as the distance between two consecutive ripple maxima). B) The Young's modulus of PLLA nanofilms in term of SPIONs concentration and (C) mass fraction ratio.

The result for purely polymeric nanofilms confirmed what previously reported for PLLA nanofilms with comparable thickness, whose Young's modulus was estimated to be around 1-2 GPa (Fujie 2013). The addition of magnetic nanoparticles in the structure resulted in a more rigid

behavior of the nanofilms. These results are in good agreement with those reported in the literature concerning freely suspended layer-by-layer nanomembranes whose mechanical properties can be significantly enhanced by the introduction of well dispersed inorganic nanoparticles (e.g. gold nanoparticles) (Jiang 2004).

**3.3 Injectability of magnetic nanofilms.** In general, free-standing magnetic nanofilms can be manipulated with syringes, injecting and ejecting multiple times without distortion (Figure 3A-E). Even after manipulation, the nanofilms spread in the suspending medium and were unfolded (Figure 3F).

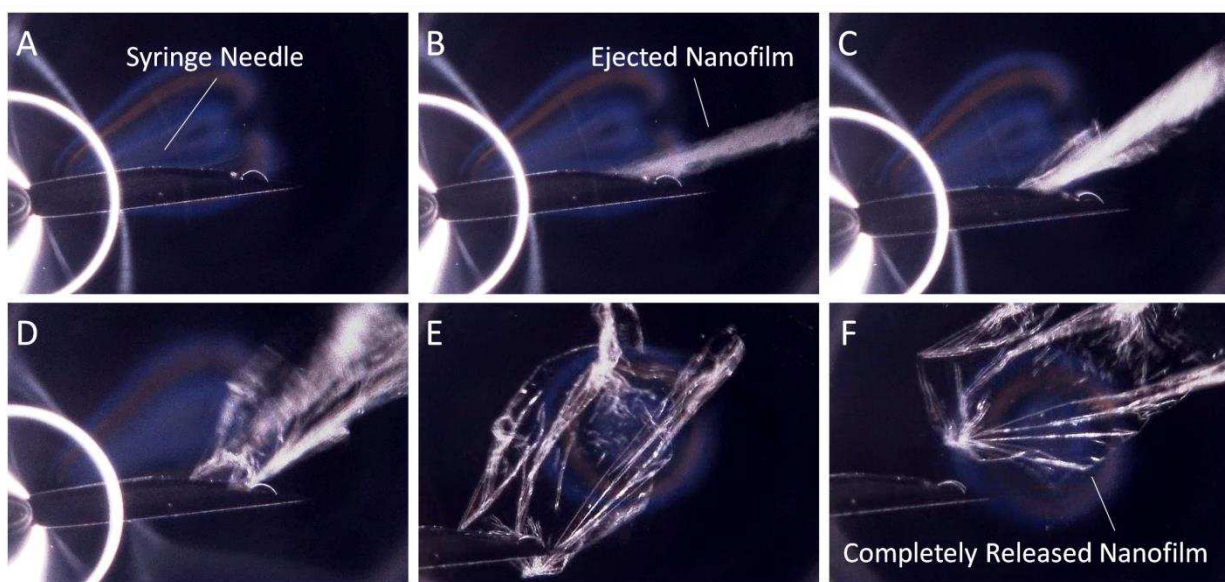


**Figure 3.** Manipulation of a PL10-SP0 nanofilm in water by a plastic syringe equipped with a needle with an inlet diameter of 1.1 mm (A): free-standing nanofilm can be ejected through the hole of the syringe (B-E) spreading in the water without damaging the structure (F).

In particular, the influence of three parameters on nanofilms injectability was investigated: lateral dimension of the nanofilms, SPIONs content and the needles diameter. For each SPIONs concentration, injectability of the magnetic nanofilms was plotted against lateral dimension of

the nanofilms (L) and needles diameter (D) (Figure 4). None of the nanofilms could be injected through the needle with an inlet diameter of 0.45 mm. Then, 0.6 mm represented the lower limit of needle diameter in the selected range.

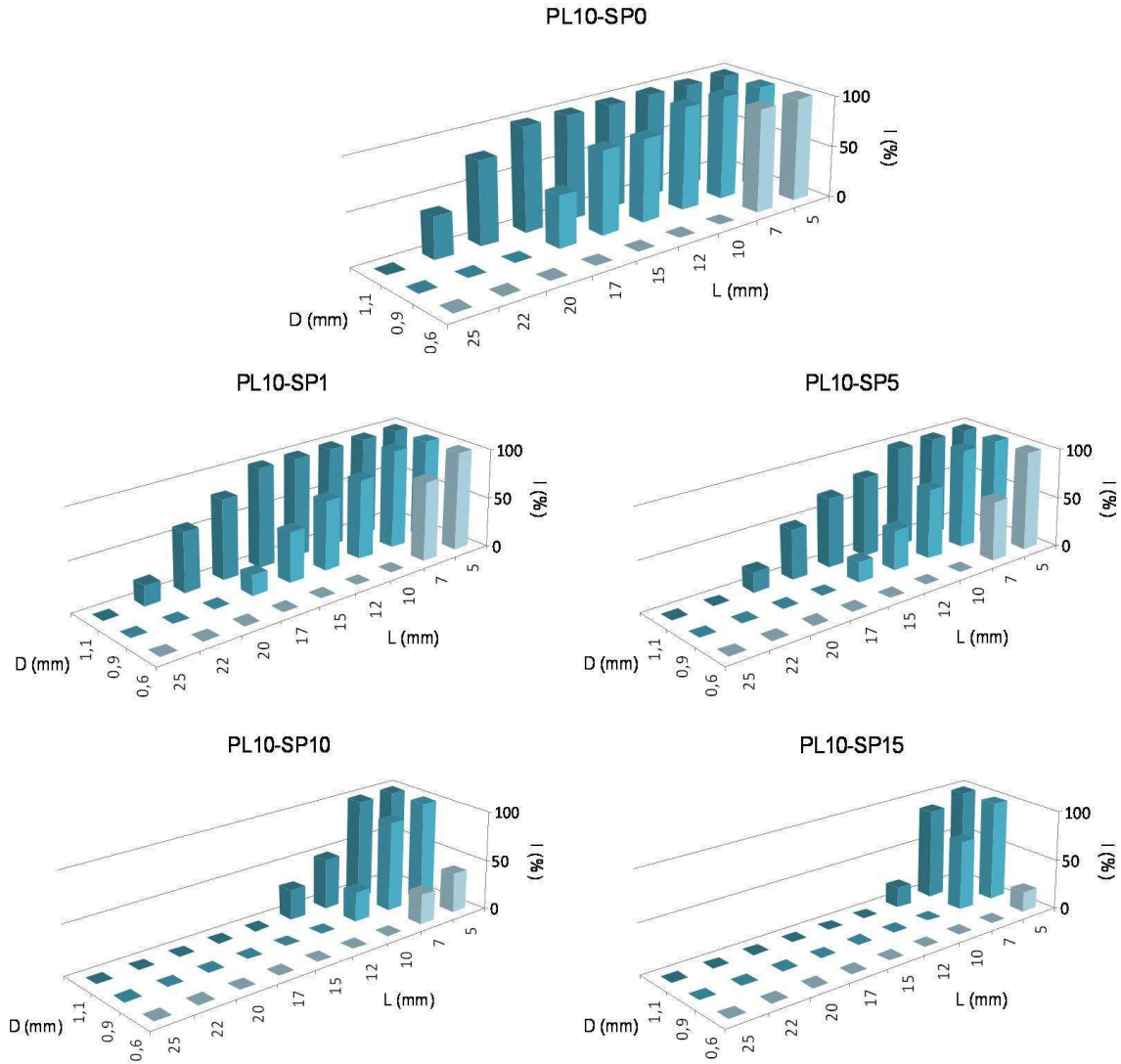


**Figure 4.** Nanofilms injectability ( $I$ ) as a function of the nanofilms lateral size ( $L$ ) and needle diameters ( $D$ ), for different SPIONs concentration.

The maximum lateral size ( $L_{max}$ ) that allowed the injection of the nanofilms without risk of rupture ( $I = 100\%$ ) in the function of SPIONs concentration and needle diameters, summarized in Table 2, is an important parameter for the practical application.

The size of the nanofilms (lateral size and thickness) played a primary role during the injection because the nanofilms with larger dimensions could cause the clogging of the needle. Therefore, the increase in the SPIONs concentration, and subsequent increase in the thickness of the nanofilms, reduced the injectability. For example, PL10-SP5 samples (thickness 140 nm) with a lateral size of 10 mm showed an injectability of 100% using 1.1 mm diameter needles, while PL10-SP15 nanofilms (thickness 205 nm), with the same lateral size, showed a lower injectability of only 20%. The incorporation of SPIONs affected not only the volume of the nanofilms but also their elastic properties making nanocomposite nanofilms less elastic deformable than purely polymeric ones and contributing to decrease the injectability. Consequently, for the same diameter of the needle and lateral size of the nanofilm, the injectability of the nanofilms decreased with increasing SPIONs concentration.

**3.4 Film injectability design.** Accordingly to experimental data, we have developed a simple model for the prediction of the injectability of films and thus for their preliminary design. Crumpling a film of lateral dimensions  $L_1$  and  $L_2$  and thickness  $h$  would lead to a ball of radius  $r$ . According to fractal laws (Carpinteri 2005) we expect a scaling in the form of  $r^d = k \cdot L_1 \cdot L_2 \cdot h$  where  $2 \leq d \leq 3$  is the fractal dimension of the crumpled ball and  $k$  is a constant (with not integer physical units). Considering  $L_1 = L_2 = L_{max}$ ,  $h$  for each type of nanofilm (Table 1),  $2r = D$  as condition of injectability (note that also  $2r$  equal to a fraction of  $D$  would lead to identical results, with different values of  $k$ ), and deducing  $k$  from the single case of  $D = 0.6$  mm and PL10-SP0,

we can compare the predictions of the model in the limiting cases of  $d = 2$  and  $d = 3$  with the experimental observations. The comparison is reported in Table 2 and shows a close agreement.

**Table 2.** Maximum lateral size  $L_{\max}$  which corresponds to an injectability of 100%. Comparison between experimental observations and model predictions (in brackets).

Sample	Maximum Lateral Size $L_{\max}$ (mm)		
	D = 0.6 mm	D = 0.9 mm	D = 1.1 mm
PL10-SP0	7 (=7)	10 (10-13)	17 (13-17)
PL10-SP1	5 (4)	7 (6-8)	15 (8-11)
PL10-SP5	5 (4)	7 (7-8)	10 (8-11)
PL10-SP10	- (4)	5 (6-7)	7 (7-10)
PL10-SP15	- (3)	5 (4-5)	5 (5-7)

**3.5 Morphology of injected films.** From a morphological point of view, observing the shape of the nanofilms immediately after the injection, nanofilms with high injectability ( $I > 70\%$ ) showed the ability to recover their shape and spread in the water more easily than low-injectable nanofilms ( $I < 70\%$ ), which tended to remain in a “crumpled state” (Figure 5A,B). The ability to recover the spreading shape is an important factor for the intended application because the crumpled state could prevent the adhesion to the tissues. For this reason, after the release, the stretch and the spread of the nanofilms could be further promoted alternating flux of water and air directly through the working channel of the endoscope or with the aid of the external magnetic field.

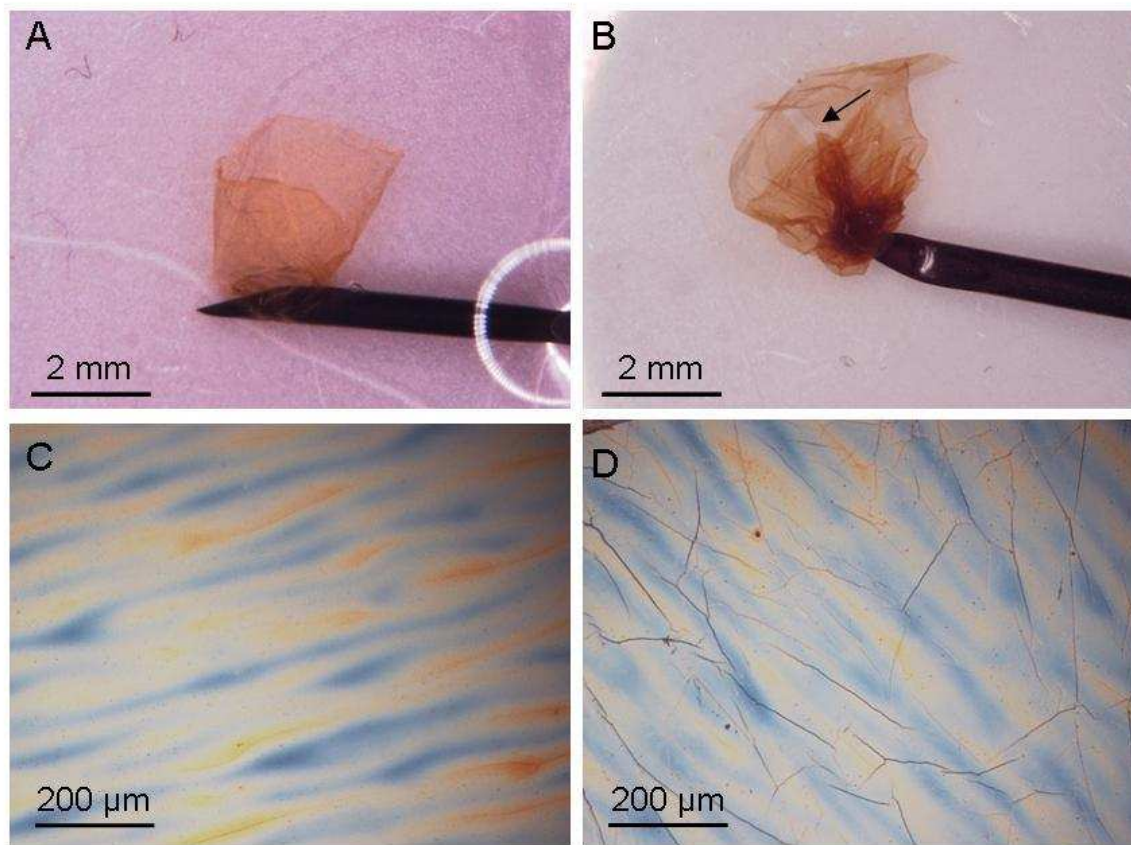


**Figure 6.** Digital optical microscope images of magnetic nanofilms during and after the injection (on nanofilms collected and dried on clean silicon wafer) through a 1.1 mm diameter needle: (A) and (C) a spread PL10-SP10 nanofilm ( $l = 7$  mm,  $I = 100\%$ ); (B) and (D) a crumpled PL10-SP15 nanofilm ( $l = 10$  mm,  $I = 20\%$ ). The arrow indicates a rupture site in the low-injectable nanofilm.

The surface of the nanofilms after the injection has been analyzed by digital optical microscopy on nanofilms collected and dried on clean silicon wafers. Crumpled nanofilms have been unfolded with the aid of tweezers and fluxes of water through the syringe and collected on silicon wafers after they have assumed the spread shape. Nanofilms with high injectability did not show showed any cracks, wrinkles or other discontinuities caused by the induced stresses (Figure 5C,D). When  $I > 70\%$ , the unaltered integrity of the structure was demonstrated also at

the micro-scale observing the surface of the nanofilms by AFM before and after the injection (Figure 6A,B).

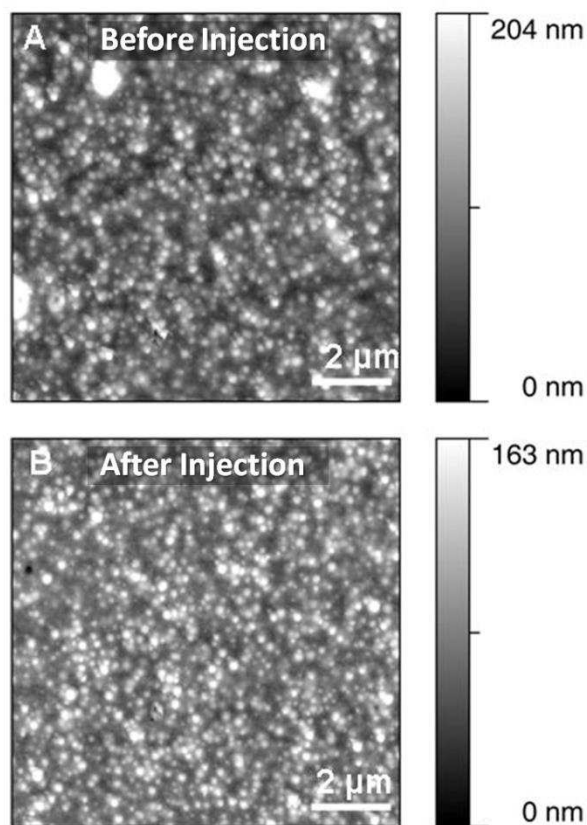


**Figure 7.** AFM surface topography of a PL10-SP10 nanofilm ( $L = 7$  mm,  $D = 0.9$  mm,  $I = 90\%$ ) before (A) and after (B) the injection.

On the other hand, low-injectable nanofilms showed not only macroscopic ruptures but also the presence of discontinuities on their surface (Figure 6D). In particular, irreversible wrinkles were formed on nanofilms' surface due to the compressive stresses that occur during the injection. The wrinkling phenomenon was observed for the samples with low injectability ( $I < 70\%$ ), independently from the content of SPIONs in the polymeric matrix.

As mentioned before, the incorporation of SPIONs makes the nanofilms thicker and less elastically deformable: in the same range of needle diameters and lateral size of the nanofilms,

the injectability of the nanofilms decreased with increasing SPIONs concentration. Consequently, at higher SPIONs concentration (i.e. SP10-10, SP10-15), the wrinkling phenomenon occurs more frequently. Also in this case, choosing the right conditions for the injection (diameter of the needle and lateral size of the nanofilm) the wrinkling phenomenon can be avoided.

#### **4. CONCLUSIONS**

The present study revealed that magnetic PLLA-SPIONs nanofilms are extremely flexible and deformable. The inclusion of polymer-coated SPIONs in a PLLA matrix, although leading to an increase in the mechanical properties of the nanofilms, kept their elastic modulus value at a considerably low value. The ability of these flexible nanofilms to be manipulated with syringes without distortion has been experimentally studied and was quantified by the injectability parameter  $I$ . An analytical model to predict the injectability threshold vs. geometrical parameters was also presented. Integrity of the nanofilm structure and ability to recover the spread shape after the ejection can be guaranteed by choosing the right combination of needle size, nanofilm lateral dimension and SPIONs content. As foreseen in previous papers these nanofilms can be manipulated and precisely positioned within the working environment by using an external magnetic field and could thus provide a novel controllable injectable support in biomedical applications.

## **ACKNOWLEDGMENT**

This work was supported in part by JFE (The Japanese Foundation for Research and Promotion of Endoscopy) Grant (T.F.). JSPS KAKENHI (grant number 15H05355 for T.F.) from MEXT, Japan, and the Precursory Research for Embryonic Science and Technology (PRESTO) from the Japan Science and Technology Agency (JST) (grant number 15655478 for T.F.). Nicola M. Pugno is supported by the European Research Council PoC 2015 "Silkene" No. 693670, by the European Commission H2020 under the Graphene Flagship Core 1 No. 696656 (WP14 "Polymer Nanocomposites") and under the FET Proactive "Neurofibres" No. 732344.

## REFERENCES

- C. Jiang, V. V. Tsukruk, *Adv. Mater.* 18, 829 (2006)
- S. S. Ono, G. Decher, *Nano Lett.* 6, 592 (2006)
- Z. Tang, Y. Wang, P. Podsiadlo, N. A. Kotov, *Adv. Mater.* 18, 3203 (2006)
- A. A. Mamedov, N. A.; Kotov, *Langmuir* 16, 5530 (2000)
- T. Fujie, *Polym. J.* 48, 773 (2016)
- C. Jiang, S. Markutsya, Y. Pikus, V. V. Tsukruk, *Nature Mater.* 3, 721 (2004)
- A. A. Mamedov, N. A. Kotov, M. Prato, D. Guldi, J. Wicksted, A. Hirsch, *Nature Mater.* 1, 190 (2002)
- E. Redolfi Riva, A. Desii, E. Sinibaldi, G. Ciofani, V. Piazza, B. Mazzolai, V. Mattoli, *ACS Nano* 8, 5552 (2014)
- F. Greco, A. Zucca, S. Taccola, A. Menciassi, T. Fujie, H. Haniuda, S. Takeoka, P. Dario, V. Mattoli, *Soft Matter* 7, 10642 (2011)
- H. Endo, Y. Kado, M. Mitsuishi, T. Miyashita, *Macromolecules* 39, 5559 (2006)
- G. Decher, *Science* 277, 1232 (1997)
- R. Vendamme, S. Onoue, A. Nakao, T. Kunitake, *Nat. Mater* 5, 494 (2006)
- Y. Okamura, K. Kabata, M. Kinoshita, D. Saitoh, S. Takeoka, *Adv. Mater.* 21, 4388 (2009)
- T. J. Kang, M. Cha, E. Y. Jang, J. Shin, H. U. Im, Y. Kim, J. Lee, Y. H. Kim, *Adv. Mater.* 20, 3131 (2008)
- E. Redolfi Riva, A. Desii, S. Sartini, C. La Motta, B. Mazzolai, V. Mattoli, *Langmuir* 29, 13190 (2013)
- S. Taccola, F. Greco, A. Zucca, C. Innocenti, C. de Julián Fernández, G. Campo, C. Sangregorio, B. Mazzolai, V. Mattoli, *ACS Appl. Mater. Interfaces* 5, 6324 (2013)

A. Zucca, C. Cipriani, S. Sudha, S. Tarantino, D. Ricci, V. Mattoli, F. Greco, *Adv Healthc. Mater.* 4, 983 (2015)

T. Fujie, Y. Okamura, S. Takeoka, *Adv. Mater.* 19, 3549 (2007)

T. Fujie, N. Matsutani, M. Kinoshita, Y. Okamura, A. Saito, S. Takeoka, *Adv. Funct. Mater.* , 19, 2560 (2009)

V. Pensabene, V. Mattoli, T. Fujie, A. Menciassi, S. Takeoka, P. Dario, *Proceedings of the 9<sup>th</sup> Nanotechnology Conference IEEE Nano; Genova* (2009)

L. Ricotti, S. Taccola, V. Pensabene, V. Mattoli, T. Fujie, S. Takeoka, A. Menciassi, P. Dario, *Biomed. Microdev.* 12, 809 (210)

T. Fujie, L. Ricotti, A. Desii, A. Menciassi, P. Dario, V. Mattoli, *Langmuir* 27, 13173 (2011)

T. Fujie, A. Desii, L. Ventrelli, B. Mazzolai, V. Mattoli, *Biomedical Microdevices* 14, 1069 (2012)

L. Ventrelli, T. Fujie, S. Del Turco, G. Basta, B. Mazzolai, V. Mattoli *J. Biomed. Mater. Res. Part A* 102, 2652 (2014)

T. Fujie, Y. Mori, S. Ito, M. Nishizawa, H. Bae, N. Nagai, H. Onami, T. Abe, A. Khademhosseini, H. Kaji, *Adv. Mater.* 26, 1699 (2014)

I. Baker, Q. Zeng, W. Li, C. Sullivan, *J. Appl. Phys.* 99, 08H106 (2006)

Z. Wang, P. André, D. McLean, S.I. Brown, G.J. Florence, A. Cuschieri, *Med. Eng. Phys.* 36, 1521 (2014)

Q. Wang, E. Chen, Y. Cai, C. Chen, W. Jin, Z. Zheng, X. Jin, Y. Chen, X. Zhang, Q. Li, *World J. Surg. Oncol.* 14, 231 (2016)

Z. Wang, L. Wang, B. Tang, T. Frank, S. Brown, A. Cuschieri, *Surg. Endosc.* 22, 1838 (2008)

V. Pensabene, P. Valdastri, S. Tognarelli, A. Menciassi, A. Arezzo, P. Dario, *Surg. Endosc.* 25, 3071 (2011)

V. Mattoli, S. Sinibaldi, V. Pensabene, S. Taccola, A. Menciassi, P. Dario, Proceedings of ICRA 2010 – 2010 IEEE International Conference on Robotics and Automation, Anchorage (Alaska, USA), 2010.

S. Taccola, A. Desii, V. Pensabene, T. Fujie, A. Saito, S. Takeoka, P. Dario, A. Menciassi, V. Mattoli, *Langmuir* 27, 5589 (2011)

G. Ciuti, R. Donlin, P. Valdastri, A. Arezzo, A. Menciassi, M. Morino, P. Dario, *Endoscopy* 42, 148 (2010)

C. M. Stafford, C. Harrison, K. L. Beers, A. Karim, E. J. Amis, M. R. Vanlandingham, H. Kim, W. Volksen, R. D. Miller, E. E. Simonyi, *Nature Mater.* 3, 545 (2004)

T. Fujie, Y. Kawamoto, H. Haniuda, A. Saito, K. Kabata, Y. Honda, E. Ohmori, T. Asahi, S. Takeoka, *Macromolecules* 46, 395 (2013)

A. Carpinteri, N. Pugno, *Nature Mater.* 4, 421 (2005)

## Table of Contents/Abstract Graphic

